Princeton Plasma Physics Laboratory

PPPL- 4852

PPPL- 4852

Particle Control and Plasma Performance in the Lithium Tokamak Experiment (LTX)

Richard Majeski, et. al.

February, 2013

Prepared for the U.S. Department of Energy under Contract DE-AC02-09CH11466.

Princeton Plasma Physics Laboratory
Report Disclaimers

Full Legal Disclaimer

Trademark Disclaimer

PPPL Report Availability

Princeton Plasma Physics Laboratory:

http://www.pppl.gov/techreports.cfm

Office of Scientific and Technical Information (OSTI):

http://www.osti.gov/bridge

Related Links:

U.S. Department of Energy

Office of Scientific and Technical Information

Fusion Links

Particle control and plasma performance in the Lithium Tokamak eXperiment (LTX)

R. Majeski, T. Abrams, D. Boyle, E. Granstedt, J. Hare, C. M. Jacobson, R. Kaita, T. Kozub, B. LeBlanc, D. P. Lundberg, M. Lucia, E. Merino, J. Schmitt, D. Stotler

Princeton Plasma Physics Laboratory, Princeton, New Jersey 08543

T. M. Biewer, J. M. Canik, T. K. Gray, R. Maingi, A. G. McLean

Oak Ridge National Laboratory, Oak Ridge, Tennesee 37831

S. Kubota, W. A. Peebles

University of California at Los Angeles, Los Angeles, California 90095

P. Beiersdorfer, J. H. T. Clementson

Lawrence Livermore National Laboratory, Livermore, California 94550

K. Tritz

Johns Hopkins University, Baltimore, Maryland 21218

Abstract. The Lithium Tokamak eXperiment (LTX) is a small, low aspect ratio tokamak,[1] which is fitted with a stainless steel-clad copper liner, conformal to the last closed flux surface. The liner can be heated to 350 °C. Several gas fueling systems, including supersonic gas injection, and molecular cluster injection have been studied, and produce fueling efficiencies up to 35%. Discharges are strongly affected by wall conditioning. Discharges without lithium wall coatings are limited to plasma currents of order 10 kA, and discharge durations of order 5 msec. With solid lithium coatings discharge currents exceed 70 kA, and discharge durations exceed 30 msec. Heating the lithium wall coating, however, results in a prompt degradation of the discharge, at the melting point of lithium. These results suggest that the simplest approach to implementing liquid lithium walls in a tokamak – thin, evaporated, liquefied coatings of lithium – does not produce an adequately clean surface.

I. Introduction

The possibility of using liquid metals as plasma-facing components (PFCs) for a fusion power plant has been discussed for decades. The Advanced Limiter-divertor Plasma-facing Systems (ALPS) program in the U.S.[2] considered engineering approaches to the implementation of liquid metal (or liquid salt) PFCs. Liquid metals constitute a viable alternative to the use of solid tungsten PFCs in a reactor. The liquid metals generally considered as candidates for PFCs are gallium, tin, and lithium.[3] Of these candidates, virtually no experimental tests of gallium or tin have been conducted in confinement devices, whereas lithium wall coatings and wall conditioning have been tested in a number of devices, and observed to strongly affect tokamak performance, since the experiments on the Tokamak Fusion Test Reactor (TFTR).[4] Several, more recent, experiments[5,6,7,8] have employed localized limiters of liquid lithium, but the liquid lithium surface area in these systems has never exceeded a few percent of the total plasma surface. Evaporation from a liquid lithium limiter at a temperature of 350 – 400 °C will coat line-of-sight PFCs with lithium, but the coating will remain solid if the PFCs are not heated to the melting point of lithium (182 °C). As a result, most of the Plasma-Material Interactions (PMI) in present experiments occur with solid, not liquid, lithium coatings on plasma-facing surfaces. The Lithium Tokamak eXperiment (LTX) was designed to investigate the modifications to tokamak confinement and equilibrium produced by a full lithium wall, either solid or liquid.

Experiments have been performed in LTX with lithium coatings on a conductive, close fitting wall consisting of a thin (1.5 mm) explosively bonded stainless steel barrier on a thick (1.0 cm) copper shell. The shell is constructed in four quadrants, with two poloidal and two toroidal gaps or breaks. It is fitted with a total of 30.5 kW of resistive electric heaters (7.6 kW per shell quadrant) to allow operation over a wide temperature range: from room temperature through the melting point of lithium to a present maximum operating temperature of 350 °C. The area of the shell is 5 m^2, or 85% of the total plasma surface area, so that the boundary and edge-plasma interactions of the discharge are determined almost entirely by the plasma-facing shell surface. The shell can be entirely coated with a thin layer of lithium by evaporation. Alternatively, the lower shell quadrants are designed so that each quadrant can be filled with 100 – 200 g. of liquid lithium. LTX is a low aspect ratio (A=1.6) tokamak, with major radius R=0.4 m, and minor radius a=0.26 m.[1] At present, the device operates with $B_{toroidal} = 2.1$ kG, $I_P < 100$ kA, and $\tau_{discharge}$

~ 30-35 msec. Discharges are limited on the conformal wall; there is no provision for diverted operation. A photograph of the interior of LTX during a vent is shown in Figure 1.

II. The effect of lithium wall coatings on LTX discharges

Much of the results obtained to date involve solid coatings of lithium on the plasma-facing surfaces of the shells. Shell coatings are applied with a simple system of evaporators, which operate with a helium gas fill of the vacuum vessel to 1-5 mTorr, to disperse the evaporated lithium evenly over the interior, plasma facing, shell surfaces. A photograph of one of the evaporator systems, after an evaporation cycle and prior to cleaning, is shown in Figure 2. The lithium coatings evident on the structure surrounding the evaporation crucible, and in the crucible itself, are removed by reacting with common white vinegar (8% acetic acid solution), which reduces the residual metallic lithium to water-soluble lithium acetate. A subsequent water rinse and baking cycle are sufficient to return the evaporation system to service, ready for a refill with approximately 8 grams of lithium metal.

With a close-fitting high-Z wall such as the LTX shell structure, discharges are strongly affected by wall conditioning. In LTX, the only wall conditioning technique used is lithium coating. The stainless steel plasma facing surface has never been coated with other low-Z materials, and there are no low-Z (carbon, boron carbide, etc.) limiters. Discharges without lithium wall coatings were limited to plasma currents of order 10 kA, and discharge durations of approximately 5 msec. With lithium coatings, discharge currents exceed 70 kA, and discharge durations exceed 30 msec, a factor of 4-5 increase in both peak current and duration. A comparison of the plasma current in a pre-lithium and a post-lithium discharge is shown in Figure 3(a). The reduction of recycling is a major factor affecting peak plasma current, although lithium coatings also reduce high-Z impurities. The time history of the vessel pressure for intervals which include a tokamak discharge, with bare stainless steel shell surfaces, and with lithium coated shells, is shown in Fig. 3(b). Without lithium coatings (red trace), the vessel pressure immediately following a discharge is higher than the prefill pressure, indicating that the wall is a particle source. With fresh lithium coatings, the vessel pressure following a discharge is significantly lower than the prefill pressure (blue trace), indicating that the wall is strongly pumping. Note that a much higher prefill pressure is required with fresh lithium coated shells. Figure 3(b) also shows the reduction in wall pumping

as the lithium coating ages, or passivates. Interestingly, the time scale for passivation is far longer than the time scale for accumulation of a monolayer on the lithium coating, which at the background pressure in LTX (generally mid 10^{-8} Torr – low 10^{-7} Torr) requires only a few tens to perhaps a hundred seconds.

An indication that the increase in plasma current (and discharge performance) with lithium coatings was due to reduced recycling was that saturation of the lithium wall coating with hydrogen affected the peak plasma current. Localized saturation of the lithium coatings with hydrogen, which generally occurred after 1-2 days of tokamak operations, resulted in a drop in peak plasma current by 30 – 40%. We found that high plasma current operation could be restored by changing fueling locations, until the lithium coatings local to the new fueling location were again saturated. Since LTX has three toroidally-separated high efficiency fueling locations, this process could be repeated once again, until the coatings local to the third (and last) fueling system are finally saturated. This highlights the need for high efficiency fueling, since low efficiency fueling results in faster saturation of the wall coatings. Note that saturation of the wall with hydrogen does not produce an impurity source, but rather additional fueling, with a high recycling wall. This result therefore supports the conclusion that good plasma performance in LTX, with a close fitting metallic wall, is highly dependent on the level of wall recycling, rather than simply requiring the reduction in impurities afforded by low-Z wall coatings.

In Figure 4, the overall fraction of the fueled gas which was pumped by the wall, per discharge, is shown, as a function of the total number of injected particles. This fraction is calculated from the measured vessel pressure immediately before, and within 100 – 150 msec after, a discharge (before the torus vacuum system can affect the pressure). In Figure 3(b), for example, the "before" pressure would be taken at approximately 0.35 – 0.4 seconds, and the "after" pressure would be taken at approximately 0.55 seconds. Freshly applied solid wall coatings of lithium are found to pump nearly 100% of the fueled particle inventory. Wall pumping degrades as the lithium coatings age over several days, as also seen in Figure 3(b), and importantly this degradation is much faster when the walls are heated above the melting point of lithium, as discussed in Section IV.

In March 2012 the LTX OH system was reconfigured to produce longer discharges (30-35 msec, twice the discharge duration on the predecessor to LTX, the Current Drive eXperiment – Upgrade, CDX-U),[9] with reduced loop voltage, in preparation for liquid lithium operation. Peak plasma current during 2012 was typically 40 – 50 kA for 30 – 35 msec discharges. Results from the LTX multipoint Thomson scattering system after this reconfiguration indicate that electron temperatures are in the 100 eV range, for discharges against solid lithium-coated PFCs.[10] Electron temperature profiles are broad and relatively flat in the core. Note that the shell is located at R=66 cm, and the axis is at R=40 cm. Passive Charge-Exchange Recombination spectroscopy (CHERs) data has also been obtained,[11,12] in a collaboration with the Oak Ridge National Laboratory, and indicates relatively high peak impurity (lithium) ion temperatures (up to ~70 eV) for a low (few × 10^{19} m^{-3}) density, Ohmic discharge. Initial ion temperature profiles from the ORNL CHERs system, along with toroidal velocity profiles, are also shown in Reference 10. The toroidal rotation velocity profiles range from 20 – 50 km/sec., and are relatively constant, decreasing by of order 10% out to the plasma half-radius.

Energy confinement time estimates have been made for several discharges, using measurements of stored energy from a compensated diamagnetic loop.[13] Confinement times for ~50 kA discharges with cold lithium wall coatings are in the 3-4 msec. range, similar to, or 20-30% in excess of, ITER98p(y,2) scaling.[14] Confinement enhancements comparable to those observed on CDX-U, where energy confinement times exceeded ITER98p scaling by 2-3 times,[9] have not yet been observed with lithium coated shells in LTX. By comparison, neutral-beam heated discharges with solid lithium wall coatings in NSTX exceeded ITER97 L-mode scaling by a factor of 2-3[15] (or, approximately, 1.4 – 2× ITER98p ELMy H-mode confinement[16]). Neutral beam heated TFTR discharges with extensive lithium coatings evidenced confinement times which exceeded L-mode energy scaling by up to a factor of 3.3.[4] Note that the LTX discharges discussed here were Ohmically heated only. There is, however, no available data on the improvement in Ohmic confinement provided by lithium wall coatings from either NSTX or TFTR, and the confinement results referenced were from discharges where neutral beam heating dominated.

A flat-field grazing-incidence grating spectrometer has been installed on LTX in collaboration with Lawrence Livermore National Laboratory. This diagnostic, the Long-Wavelength Extreme

Ultraviolet Spectrometer (LoWEUS),[17] has the same characteristics as a similar instrument used on the National Spherical Torus eXperiment, NSTX. LoWEUS employs a variable space grating with an average spacing of 1200 lines/mm and covers 90–270 Å wavelength band. With a line width (FWHM) of ~0.3 Å, the spectrometer is able to resolve Lyman-α lithium lines, L-shell lines of oxygen, and K-shell lines of carbon. Initial spectra from LoWEUS in LTX plasmas with cold lithium wall coatings indicate the presence of OIV, OV, and OVI lines, which are also consistent with the measured core electron temperature of approximately 100 eV. The EUV spectra shown in Figure 9 (a and b) were obtained with the LoWEUS instrument.

In addition, numerous "filterscopes" are installed on LTX, to monitor visible edge emission from impurity species. Examples of oxygen II and H_α data taken with the filterscope system during the hot wall experiments are shown in Figures 11 and 12.

III. Gas fueling experiments in LTX

LTX discharge fueling employs gas injection of hydrogen. Hydrogen is used rather than deuterium, in part because neutral beam injection is planned for LTX in the near future, and the production of beam-target neutrons with a deuterium beam and target plasma must be avoided for safety reasons. Except for the discharge prefill, where the fueling efficiency is independent of the gas injection technique, discharge fueling employs various types of directed gas jets, in an attempt to increase the discharge fueling efficiency, and minimize the edge neutral gas over most of the plasma surface area. We have now studied the fueling efficiency of gas injection techniques, including a simple pulsed gas valve mounted on the chamber wall, a pulsed valve with a gas duct a supersonic gas injection (SGI), and molecular cluster injection (MCI).[18,19] With the exception of the wall-mounted pulsed valve, which is mounted at the top of the vacuum chamber, and injects gas through a 3" diameter aperture in one of the shell quadrants, all the fueling systems are on the outboard midplane of the device. In LTX, a simple wall mounted valve is found to fuel the plasma with approximately 15% efficiency; the plasma density rise seen during gas injection indicates that 15% of the injected gas accounts for the rise in the total plasma particle count. This is a higher fueling efficiency than typically seen with wall mounted gas valves, even with comparable plasma size (e.g. CDX-U),[20] and may be due to the close fitting shell surrounding the LTX plasma. The use of directed gas jets results in higher fueling

efficiencies. Fueling efficiency rises to 20-25% with the use of a simple tube or duct, 0.5" in diameter, leading from the valve to within 2 cm of the last closed flux surface. Directed gas jets, produced by the SGI or the MCI operated at room temperature, and molecular cluster injection with the MCI operated at liquid nitrogen temperatures, produce higher fueling efficiencies, up to 30-35% (see Fig. 5). The highest fueling rates are obtained with the MCI system precooled to cryogenic temperatures to fuel, at least partly, with condensed clusters of hydrogen molecules. The MCI system also permits greater standoff of the valve and collimation system from the edge of the plasma than is possible with the SGI.[19] The achieved efficiencies of ~35% approach the fueling efficiency obtained with low field side pellet fueling. A summary plot of fueling efficiency vs. particle flux is shown in Figure 5.

IV. Lithium coatings on hot walls

Tests of the effects of lithium coatings on hot (up to 325 °C) walls were also performed. This approach to liquid lithium walls is probably the simplest to implement. The same coating systems employed for solid coating experiments can be employed, except that the walls are heated to a temperature above the melting point of lithium, either during or following the evaporation sequence. A disadvantage of this approach is that the very thin coating which results cannot be stirred or mixed in any way, and are subject to surface accumulations of hydrogen and other impurities. A reactor implementation of liquid lithium PFCs would necessarily involve flow, which would mix any surface layer into the bulk liquid.

In the first test, an evaporation of a total of four grams of lithium onto cold walls was performed, followed immediately by plasma operations to characterize plasma performance with a cold, fresh coating of lithium. 48 hours later, another 4 grams of lithium was evaporated onto the shells, which had been preheated to 300 °C. The evaporation was followed again by immediate plasma operations. It was found that liquefied lithium coatings on a hot shell did not produce comparable gains in discharge performance, when compared to solid lithium coatings on a room-temperature wall. Although the discharges run against hot lithium coated shells had variable performance, in all cases the hot wall discharges performed poorly as compared to discharges with cold, solid walls. In Figure 4, hot-wall discharges are indicated by a red "x"; the wall is seen to either modestly pump or modestly recycle.

During evaporation onto a hot shell, visual observation of the wall coatings indicated that the coatings were rapidly passivated (reacted with residual gases). This was evidenced by the dark coloration of the wall coatings deposited during hot wall operation, which indicates the rapid formation of hydroxide coatings, although the coatings probably consisted of a mixture of compounds. A photograph of the interior of LTX, showing the coloration of the lithium wall coatings just prior to plasma operations with heated 300 °C shells, is shown in Figure 6. One possible source of the lithium coatings was reaction with water vapor and other impurities resulting from outgassing of the vessel interior due to heating, during hot shell operation at 300 °C. A residual gas analysis (RGA) trace recorded during the hot wall experiment is shown in Figure 7. The primary background gas is hydrogen, with a partial pressure 5-10× less than the typical prefill pressure for a discharge. Other background gases (e.g. water) are present at a higher level than typically seen during operation with a cold lithium wall. As a result, during this first experiment it was unclear whether poor discharge performance with hot walls, and a molten lithium film, was simply due to degraded vacuum conditions.

In subsequent experiments, the performance of discharges run against the lithium-coated shells was evaluated as a function of the shell temperature, rather than a simple comparison of performance with room temperature and 300 °C shells. This experiment was performed after a total of 100 g of lithium was applied to the shell interiors as coatings, over a period of several months, and immediately after an additional 18 grams of lithium fill (9 grams per shell quadrant) was loaded into the two lower shell quadrants. The additional lithium formed localized pools in the lower shell, approximately 8-10 cm in diameter, and several millimeters thick. We note that following this experiment LTX was vented. Examination of the localized pools showed that the surface of the lithium in the pools was coated with a thin layer of oxides and hydroxides, but beneath this surface layer virtually all the lithium remained metallic, even after the venting process.

Figure 8 is a plot of the peak plasma current obtained as a function of the wall temperature, for a large number of discharges, during this experiment. These discharges were operated with reduced loop voltage and a longer pulse length. A clear reduction in the peak plasma current is seen as the wall is heated approximately above the melting point of lithium. A clear increase in

the peak plasma current is also seen as the wall is allowed to cool below the melting point of lithium. The temperature measurement is obtained from an average of 30 thermocouples located on the outer surface of the shells, since it was not possible to reliably attach thermocouples to the inner, plasma-facing surface of the shells. As a result, the temperature at which the transition in discharge behavior occurs is consistent for both heating and cooling curves, but the transition temperature, measured at the outer shell wall, is slightly below the actual melting point of lithium, at 182 °C. This discrepancy is due to the fact that the entire inner surface of the shell faces a hot surface, as opposed to the outer surface of the shell, which radiates to the cooled vacuum vessel at a temperature of 15 °C. The difference in radiative equilibrium results in a difference in surface temperature between the inner and outer shell surfaces, which is negligible at room temperature, and estimated to be over 20 °C at 300 °C, depending on the exact thermal emissivities of the inner and outer shell surfaces, and the inner wall of the vacuum vessel.

Reliable Thomson scattering data was not available for this series of discharges. However, we see that the difference in the extreme ultraviolet (EUV) emission spectrum for a discharge just below the melting point of lithium, and at or just above the melting point of lithium is more pronounced than the difference in plasma current, and is shown in Figure 9 (a and b). Here (a) and (b) correspond to the discharges marked in Figure 8. Both discharges were run as the shell system cooled, with a benchmark (outer shell surface) thermocouple reading of 146 °C for (a) and 169 °C for (b). For discharge (b), the inner shell surface is estimated to be slightly above the melting point of lithium, whereas for discharge (a) the inner surface should be below the melting point. Note that the discharge denoted by (b) occurred earlier in time than the discharge denoted by (a), since the shells were continuously cooling during this phase of the experiment. The EUV spectrum in Figure 9(a) indicates emission from relatively high ionization states, with significant emission lines from oxygen V and VI. In contrast, the spectrum in Figure 9(b) is devoid of emission lines, indicating a much lower electron temperature for this discharge. This emission spectrum was typical of all discharges run with the shells at or above this temperature.

The LTX vacuum conditions during this experiment were considerably improved, compared to the earlier hot shell experiment. Active bakeout and cooling of the vacuum vessel had been implemented, which limited the evolution of impurities from the vessel wall during hot shell operation. RGA spectra taken at times corresponding to the discharges marked (a) and (b) in

Figures 8 and 9 show no significant differences, as shown in Figure 10 (a and b). Note that, similar to the RGA trace shown in Figure 6, the primary background gas is hydrogen – but in this case the partial pressure of hydrogen is reduced by two orders of magnitude, to the low 10^{-7} Torr range, for both discharges. Other impurity gases are only present at very low levels, in the mid to low 10^{-9} Torr range. The difference in discharge performance clearly cannot be attributed to degradation of background vacuum conditions for discharge (b) compared to discharge (a); there is little difference in the vacuum conditions for the two discharges.

Emission from low ionization states of oxygen and other impurities indicate that the degraded discharge performance above the melting point of lithium may be due to a difference in impurity influx into the discharge for solid and molten lithium wall coatings. A comparison of the visible emission from oxygen II, for the discharges noted (a) and (b) in Figure 8, is shown in Figure 11. Edge impurity emission is of course dependent on the edge electron density and temperature, and it is clear from Figure 9 that the core electron temperature was markedly different in the two discharges. Therefore, for the comparison of oxygen II emission shown in Figure 11, the emission was normalized by the ratio of the plasma stored energy for the two discharges, or approximately the volume integral of ($n_e \times T_e$). The stored energy for the discharge against a solid coating of lithium exceeded the stored energy for the discharge against the liquefied coating by a factor of 3.2. The absolute level of oxygen emission in the two discharges thus differs by over a factor of 5, even without the normalization for stored energy. This result indicates that the impurity influx was significantly reduced as the lithium shell coatings solidified (moving from discharge “b” to discharge “a” as the shells cooled). Carbon II light shows a similar normalized enhancement for hot shell operation. A reliable estimate of the core value of Z-effective for these discharges is not available, but a visible bremsstrahlung measurement (centered at 527 nm with a full-width half-maximum of 4.5 nm) indicated a (normalized) factor of 3.3 increase in emission for the discharge against the liquefied coating.

Diagnostics for neutral hydrogen density in LTX include spectroscopic measurements of both H_α and Lyman-α lines. A comparison of H_α emission from the high field side surfaces of the lithium coated shell, for discharges “a” and “b”, is shown in Figure 12. The signal intensity is also normalized to the plasma stored energy; both discharges had similar prefills and fueling. Note that the background hydrogen density with hotter shells is only slightly higher - 1.8×10^{-7}

Torr, compared to 1.5×10^{-7} Torr for lower shell temperature (Figure 10). However, neutral density in the plasma edge is significantly higher for the discharge operated against the hotter shells.

V. Discussion

LTX is the first tokamak to operate with a full, lithium-coated, conformal, high-Z wall, which can be uniformly heated to well above the melting point of lithium, to evaluate discharges with both solid and liquefied lithium walls. Plasma performance with an uncoated stainless steel wall is poor and impurity dominated. The application of lithium coatings to a cold wall, at the beginning of a 2-3 day run campaign, greatly improves plasma performance. Similar improvements have been seen in NSTX with solid lithium wall coatings.[21] However, the confinement enhancement, compared to ITER98P scaling, or the absolute level of energy confinement time (up to 6 msec [9]) seen on CDX-U with continuous lithium coatings has yet not been achieved on LTX, with once-a-day lithium coatings.

As a first step in the investigation of plasma performance with liquefied lithium walls, the conformal walls, or shells, in LTX were coated with lithium, and discharge behavior was documented as a function of the shell temperature. Plasma performance with heated shells suggests that impurities retained by thin-film liquid metal PFCs may be much more readily removed by PMI than impurities retained in the same material after solidification. This was especially demonstrated by the effect of lithium solidification on plasma performance during the cooling phase of the hot shell experiment. It has been previously observed in laboratory experiments that dissolved oxygen will segregate to the surface of liquid lithium.[22] The LTX results suggest that, along with oxygen, either the surface hydrogen concentration is enhanced as well, or alternatively hydrogen retention is reduced (recycling is increased) as lithium is heated above the melting point. As the lithium coatings are cooled through the solidus, the availability of impurities for removal by PMI appears to be reduced. The mechanism for this reduction is unclear, but one candidate is subduction of impurity atoms into the solidifying coating.

It should be noted that LTX had a long operating phase prior to this experiment, spanning over a year under vacuum. The vessel base pressure and various occasional air leaks over this time

period provided sufficient oxygen influx to allow a significant accumulation of oxygen in the lithium coating, although the exact oxygen concentration in the lithium film could not be determined. The impurity concentration in the lithium film coating the shell interior was likely to be significant, if the entire thickness of the film participated in oxygen gettering. Thin lithium films such as were employed in this experiment cannot be stirred to mix surface impurities into the bulk liquid metal. A flowing lithium PFC, such as would be necessary in a reactor implementation, or a stirred lithium pool, such as used in CDX-U, would not necessarily suffer the same impurity issue. Experiments commencing in early 2013 in LTX will employ a stirred liquid lithium pool as a plasma limiting surface, in combination with continuous coating of the upper shells via evaporation from the lithium pool.

VI. Conclusions

Operation of the LTX tokamak with solid, room temperature coatings of lithium covering 85% of the walls has produced Ohmic discharges with confinement times which match or slightly exceed ITER98p(y,2) ELMy H-mode confinement scaling. The performance improvement in these discharges is related both to a reduction of high Z impurities in the discharge, and to a reduction of recycling. Lithium coatings are found to produce an absorbing wall, which pumps virtually all of the particle inventory of a discharge. Pumping walls in LTX are combined with efficient fueling techniques which employ collimated gas jets to further reduce the neutral particle inventory at the plasma edge.

Initial experiments with PFCs coated by liquefied thin films of evaporated lithium have also been performed. These experiments indicate that the inventory of impurities pumped by the lithium film is much more readily sputtered by the edge plasma, when the film is liquefied. The observation that impurity influx is reduced when the film is resolidified also indicates that background vacuum conditions are not responsible for surface deposits of impurities in the lithium coating, but that impurities absorbed into previously deposited layers of lithium, or from the underlying stainless steel wall, while sequestered in solid lithium, segregate to the surface when the lithium is liquefied. The results suggest that any successful approach to employing clean, metallic liquid lithium as a PFC must incorporate flow, or alternatively in-situ stirring, to

eliminate such surface segregation, by mixing. Future experiments in LTX will therefore concentrate on stirred liquid lithium systems as PFCs.

VII. Acknowledgments

This work supported by USDoE contracts DE-AC02-09CH11466 and DE-AC05-00OR22725.

References

[1] R. Majeski, L. Berzak, T. Gray, R. Kaita, T. Kozub, F. Levinton, D. P. Lundberg, J. Manickam, G. V. Pereverzev, K. Snieckus, V. Soukhanovskii, J. Spaleta, D. Stotler, T. Strickler, J. Timberlake, J. Yoo, L. Zakharov, Nucl. Fusion **49**, 055014 (2009).

[2] J. N. Brooks, J. P. Allain, R. Bastasz, R. Doerner, T. Evans, A. Hassanein, R. Kaita, S. Luckhardt, R. Maingi, R. Majeski, N. B. Morley, M. Narula, T. Rognlein, D. Ruzic, R. Stubbers, M. Ulrickson, C.P.C. Wong, D. Whyte, A. Ying, Fusion Sci. Tech. 47, 669 (2005).

[3] R. Majeski, in Plasma Interaction in Controlled Fusion Devices: 3rd ITER International Summer School, edited by S. Benkadda, AIP Conf. Proc. **1237,** 122 (2010).

[4] D. K. Mansfield, D. W. Johnson, B. Grek, H. W. Kugel, M. G. Bell, R. E. Bell, R. V. Budny, C. E. Bush, E. D. Fredrickson, K. W. Hill, D. L. Jassby, R. J. Maqueda, H. K. Park, A. T. Ramsey, E. J. Synakowski, G. Taylor, G. A. Wurden, , Nucl. Fus. **41**, 1823 (2001).

[5] S. V. Mirnov, V. B. Lazarev, S. M. Sotnikov, T-11M Team, V. A. Evitkhin, I. E. Lyublinski, A. V. Vertkov, Fus. Eng. Design **65**, 455 (2003).

[6] R. Kaita, R. Majeski, T. Gray, H. Kugel, D. Mansfield, J. Spaleta, J. Timberlake, L. Zakharov, Phys. Plasmas **14**, 056111 (2007).

[7] V. Pericoli-Ridolfin, M. L. Apicella, G. Mazzitelli, O. Tudisco, R. Zagorski, FTU Team, Plasma Phys. Contr. Fusion **49**, S123 (2007).

[8] S. Mirnov, J. Nucl. Mater. **390-391**, 876 (2009).

[9] R. Majeski, R. Doerner, T. Gray, R. Kaita, R. Maingi, D. Mansfield, J. Spaleta, V. Soukhanavskii, J. Timberlake, L. Zakharov, Phys. Rev. Lett. **97**, 075002 (2006).

[10] R. Majeski, T. Abrams, L. R. Baylor, L. Berzak, T. Biewer, D. Bohler, D. Boyle, M. Cassin, E. Granstedt, T. Gray, J. Hare, C. M. Jacobson, M. Jaworski, R. Kaita, T. Kozub, B. LeBlanc, D. P. Lundberg, M. Lucia, R. Maingi, E. Merino, A. Ryou, E. Shi, J. Schmitt, J. Squire, D. Stotler, C. E. Thomas, K. Tritz, L. Zakharov, Proc. 24th IAEA Fusion Energy Conference, San Diego, 2012, paper ICC/P5-01.

[11] T. K. Gray, T. M. Biewer, D. P. Boyle, E. M. Granstedt, R. Kaita, R. Maingi, R. Majeski, Rev. Sci. Instrum. **83**, 10D537 (2012).

[12] T. M. Biewer, D. P. Boyle, T. K. Gray, R. Kaita, R. Maingi, R. Majeski, "Initial measurements of Li III dynamics in the Lithium Tokamak Experiment", Proc. 39th EPS Conf. on Plasma Physics, Stockholm, Sweden 2-6 July 2012.

[13] L. E. Zakharov and V. D. Shafranov, in *Reviews of Plasma Physics*, edited by M. A. Leontovich (Consultant Bureau, New York, 1986), Vol. 11, p. 153.

[14] O. J. W. F. Kardaun, in *Proceedings of the Eighteenth IAEA Fusion Energy Conference, Sorrento, 2000* (IAEA, Vienna, 2001), CD-ROM file ITERP/04 (unpublished).

[15] R. Maingi, S.M. Kaye, C. H. Skinner, D. P. Boyle, J. M. Canik, M. G. Bell, R. E. Bell, T. K. Gray, M. A. Joworski, R. Kaita, H. W. Kugel, B. P. LeBlanc, D. K. Mansfield, T. H. Osborne, S. A. Sabbagh, V. A. Soukhanovskii, Phys. Rev. Lett. **107**, 145004 (2011).

[16] S. M. Kaye, ITER Confinement Database Working Group, Nucl. Fusion **37**, 1303 (1997).

[17] J. H. T. Clementson, P. Beiersdorfer, E. W> Magee, D. A> Layne, R. Kaita, R. Majeski, R. Barnsley, Proc. 19th Top. Conf. on High Temperature Plasma Diagnostics, Monterey, CA 6-10 May 2012.

[18] D.P. Lundberg, R. Kaita and R. Majeski, Nucl. Fusion **52,** 013016 (2012).

[19] D. P. Lundberg, Ph. D thesis, Princeton University, Princeton, 2012.

[20] T. G. Gray, Ph. D thesis, Princeton University, Princeton, 2008.

[21] H. W. Kugel, D. Mansfield, R. Maingi, M. G. Bell, R. E. Bell, J. P. Allain, D. Gates, S. Gerhardt, R. Kaita, J. Kallman, et al., Journal Nucl. Mater. **390-391**, 1000 (2009).

[22] R. Bastasz and J. A. Whaley, Fus. Eng. Des. **72** (2004) 111-119.

Figure Captions

Figure 1. Photograph (through a fish-eye lens) of the interior of LTX during a vent, with labels for a number of the in-vessel components.

Figure 2. One of the LTX evaporator crucibles after initial use. 2 evaporators, 180° apart toroidally, are installed. Each crucible is typically filled with 8 grams of lithium. Typically a total of 4 grams of lithium is used per evaporation. The crucibles are ceramic yttria, and are not attacked by liquid lithium at temperatures up to 600 °C. The two wirelike projections into the white ceramic yttria crucible are thermocouples. The bandlike structure surrounding the crucible is a tantalum strip heater, with outer heat shields. The crucible is installed on a bellows-sealed linear motion feedthrough which allows insertion of the evaporation crucible through a gate valve mounted on LTX, into the volume enclosed by the shells.

Figure 3. (a) Discharge current pre- (blue trace) and post- (green trace) 5 g of lithium wall coatings in LTX. The prefill was increased for the post-lithium discharge (see Fig. 3b), but all other field programming was identical for the two discharges. (b) Time history of the neutral pressure before and after several discharges in LTX, with various wall conditions. The discharge start and end are denoted by the vertical red dotted lines. Note that the pressure gauge is connected to the main vessel by a duct, which significantly slows the time response of the system.

Figure 4. The fraction of the total number of injected hydrogen atoms which are pumped, per discharge, by the LTX wall, under various conditions. A negative fraction implies that the wall is a source of particles, rather than a sink.

Figure 5. Summary plot of fueling efficiency vs. fueling rate for the systems tested in LTX. The highest fueling efficiencies are obtained for the SGI and the MCI. The “top puffer” is a conventional wall-mounted piezoelectric gas valve. The “side puffer” is also a piezoelectric valve system, but it is more closely coupled to the vacuum chamber, and gas is ducted from the valve to the plasma edge through a short 2 cm diameter tube.

Figure 6. Photograph of the hot (300 °C) shells, immediately after coating with lithium. The photograph was taken through a glass viewport. The brownish coloration is indicative of a reacted (oxidized, hydroxided) lithium surface.

Figure 7. Residual gas analyzer trace taken during the first hot wall experiment. Hydrogen is the dominant background gas, but other components are present at the level of a few × 10^{-6} Torr.

Figure 8. Evolution of the plasma current with temperature. Discharges run during the shell heating cycle are in red; discharges run as the shell was cooling are indicated in blue. The heating experiment ran over a three day period. In the figure, a "." denotes a discharge on the first day of the experiment, a "+" denotes a discharge on the second day of the heating cycle, a "□" denotes a discharge on the third day of the heating cycle. Discharges during the shell cooldown all occurred on one day. Note that the temperatures are referenced to the outer surface of the shell, rather than the inner, plasma-facing surface. Discharges against walls which are heated above the melting point of lithium show a marked degradation compared to discharges run against walls just below the melting point. Two discharges are indicated in the plot – discharge "a" was run with the plasma-facing surface just below the melting point of lithium, and discharge "b" with the plasma-facing surface just above the melting point, when the temperature is corrected for the thermocouple location.

Figure 9. (a) EUV emission spectrum for a discharge with the wall just below the melting point of lithium (marked "a" in Figure 8), and (b) EUV emission spectrum for a discharge with the wall just above the melting point of lithium (marked "b" in Fig. 8). No emission lines are seen for a molten wall film.

Figure 10. (a) RGA trace taken with the wall temperature below the lithium melting point (following the discharge marked "a" in Fig. 8), and (b) just above the melting point of lithium (following the discharge marked "b" in Fig. 8). The traces are substantially identical.

Figure 11. Oxygen II emission, normalized to the plasma stored energy, for the two discharges discussed in connection with Figures 8-10.

Figure 12. H-α emission, normalized to the plasma stored energy, for the two discharges discussed in connection with Figures 8-11.

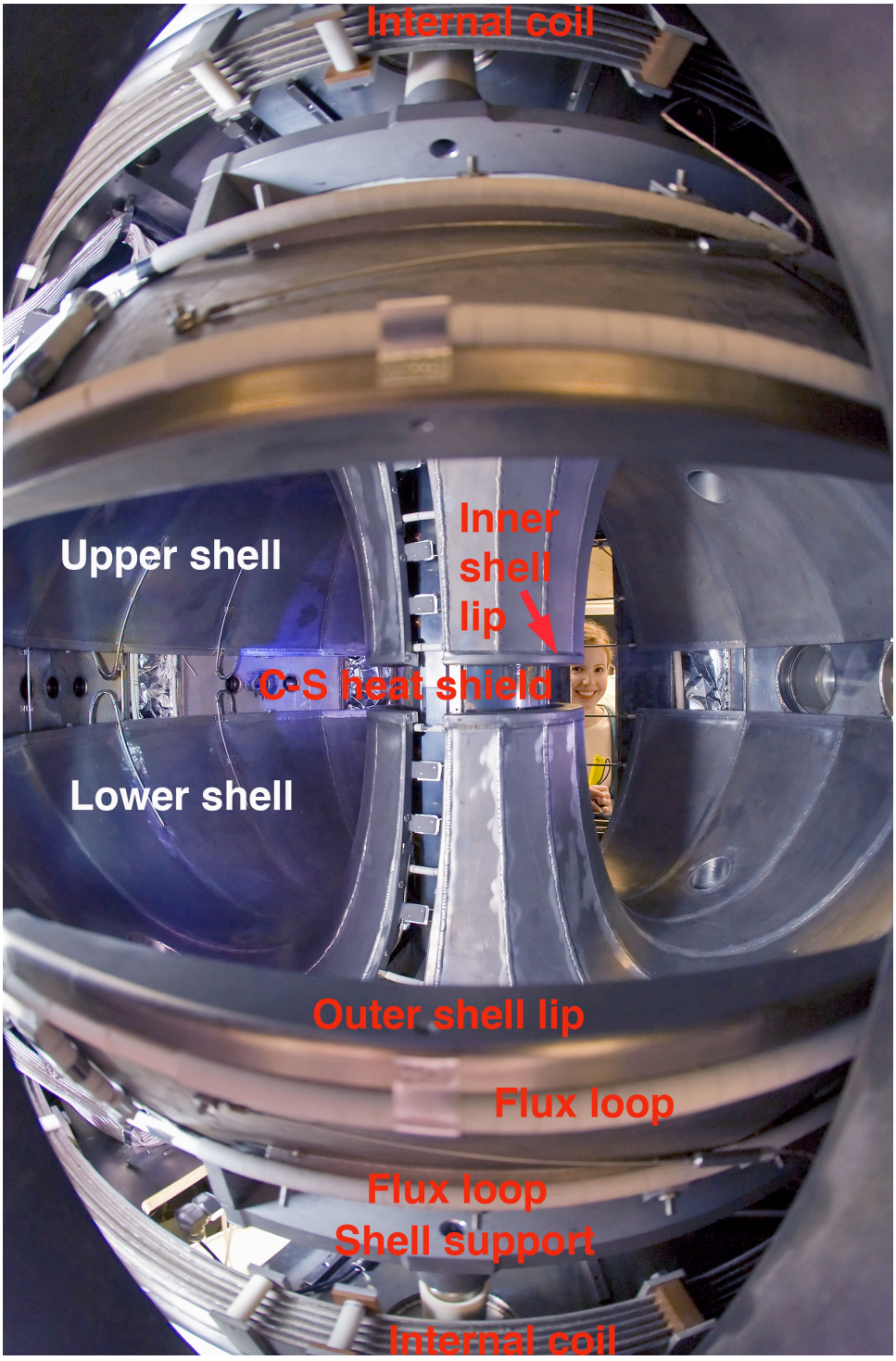
Internal coil
Upper shell
Inner shell lip
C-S heat shield
Lower shell
Outer shell lip
Flux loop
Flux loop
Shell support
Internal coil

Figure 1

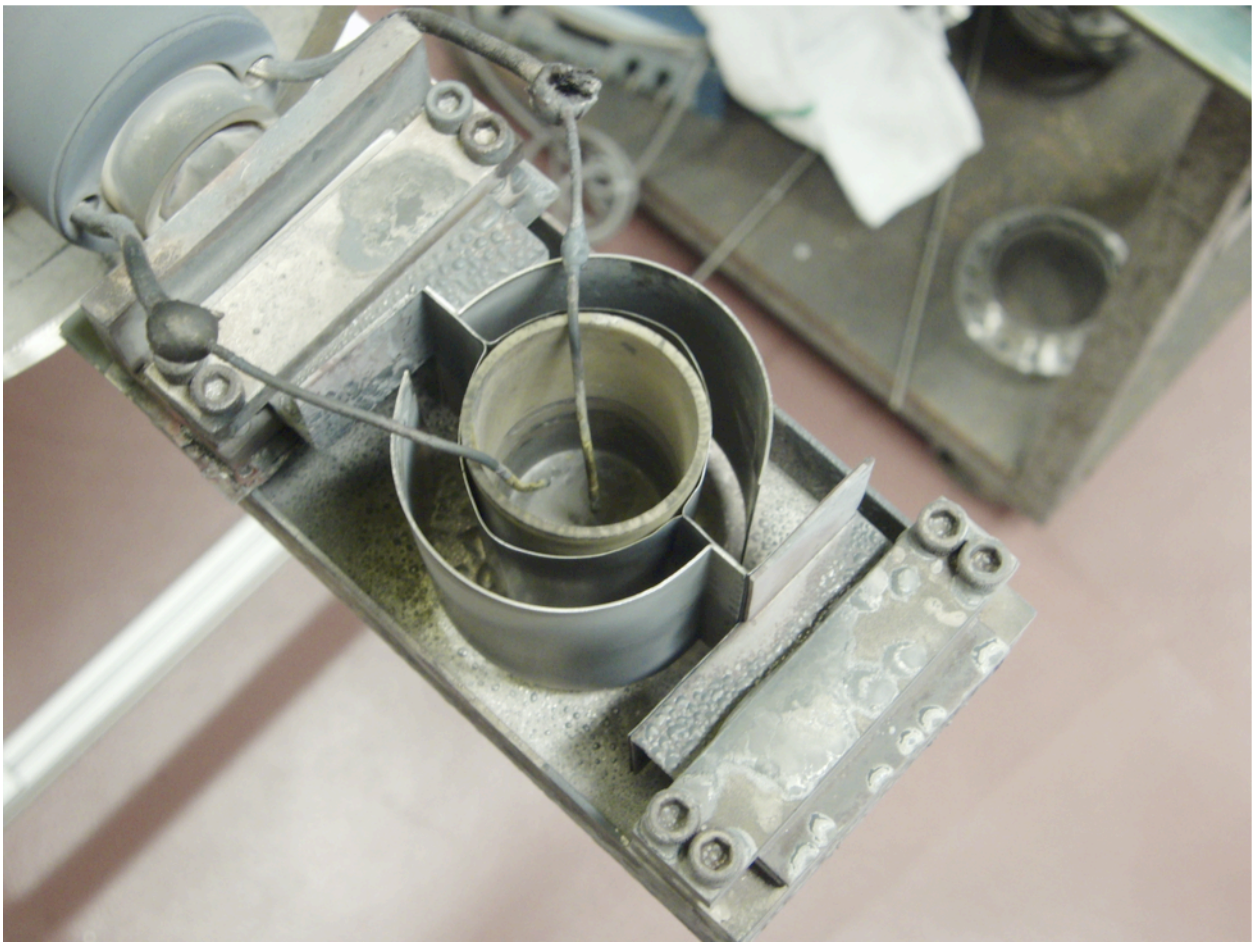

Figure 2

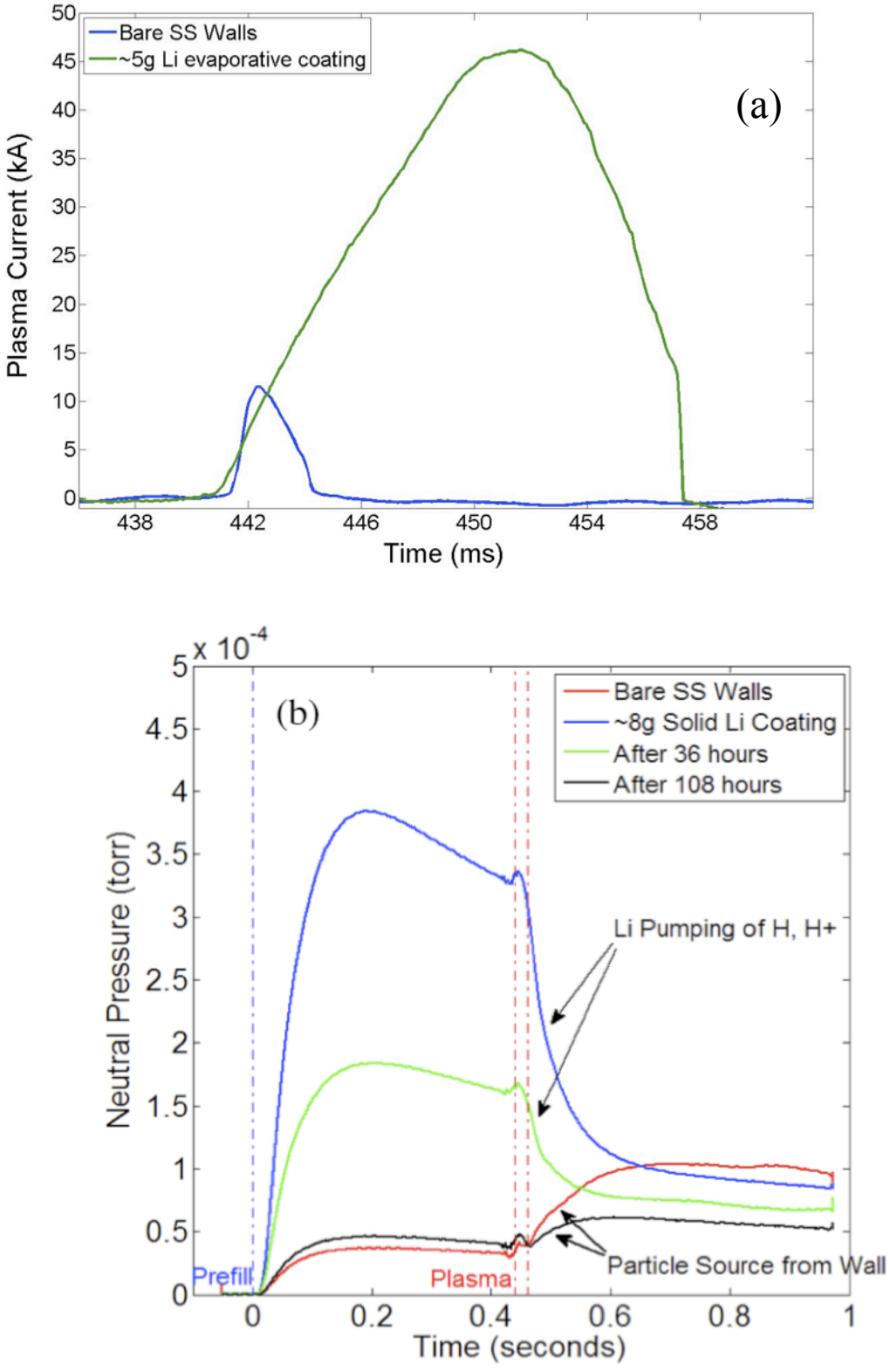
Bare SS Walls
~5g Li evaporative coating
(a)
Plasma Current (kA)
Time (ms)
x 10^-4
(b)
Bare SS Walls
~8g Solid Li Coating
After 36 hours
After 108 hours
Li Pumping of H, H+
Particle Source from Wall
Prefill
Plasma
Neutral Pressure (torr)
Time (seconds)

Figure 3

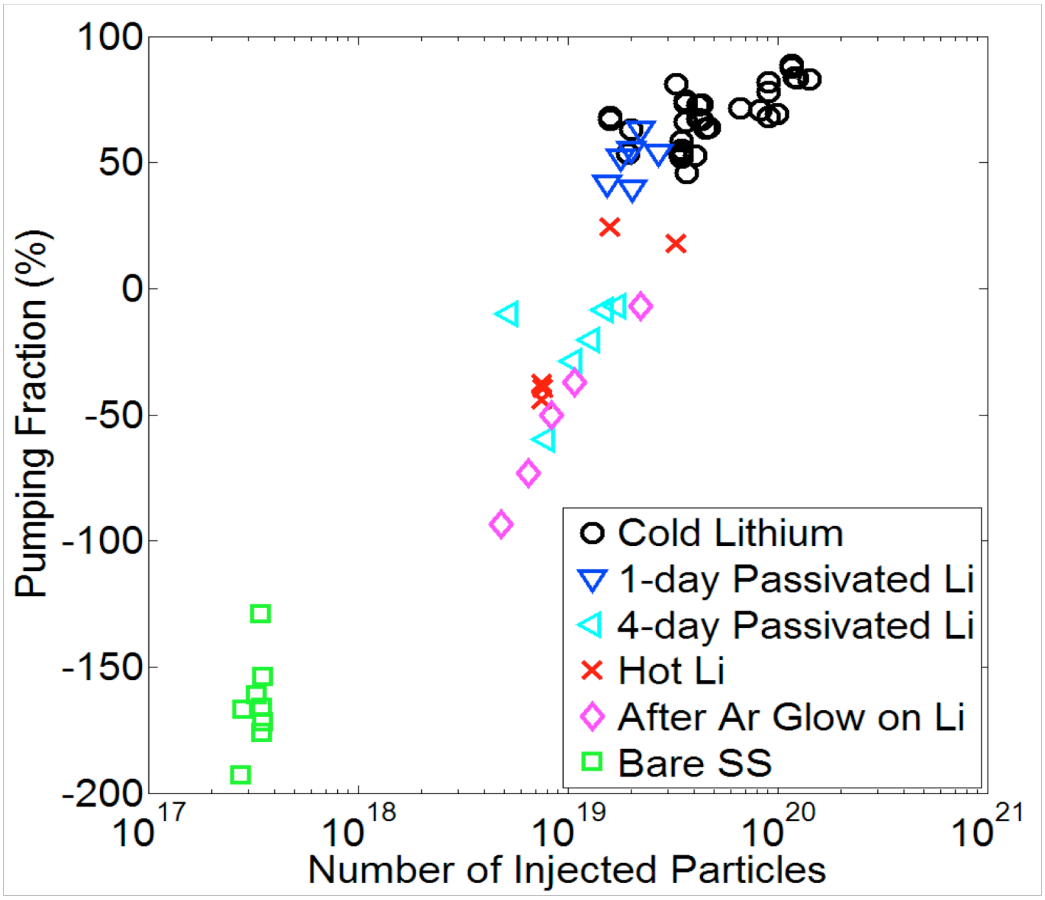
100
50
0
-50
-100
-150
-200
Pumping Fraction (%)
10^{17}
10^{18}
10^{19}
10^{20}
10^{21}
Number of Injected Particles
Cold Lithium
1-day Passivated Li
4-day Passivated Li
Hot Li
After Ar Glow on Li
Bare SS

Figure 4

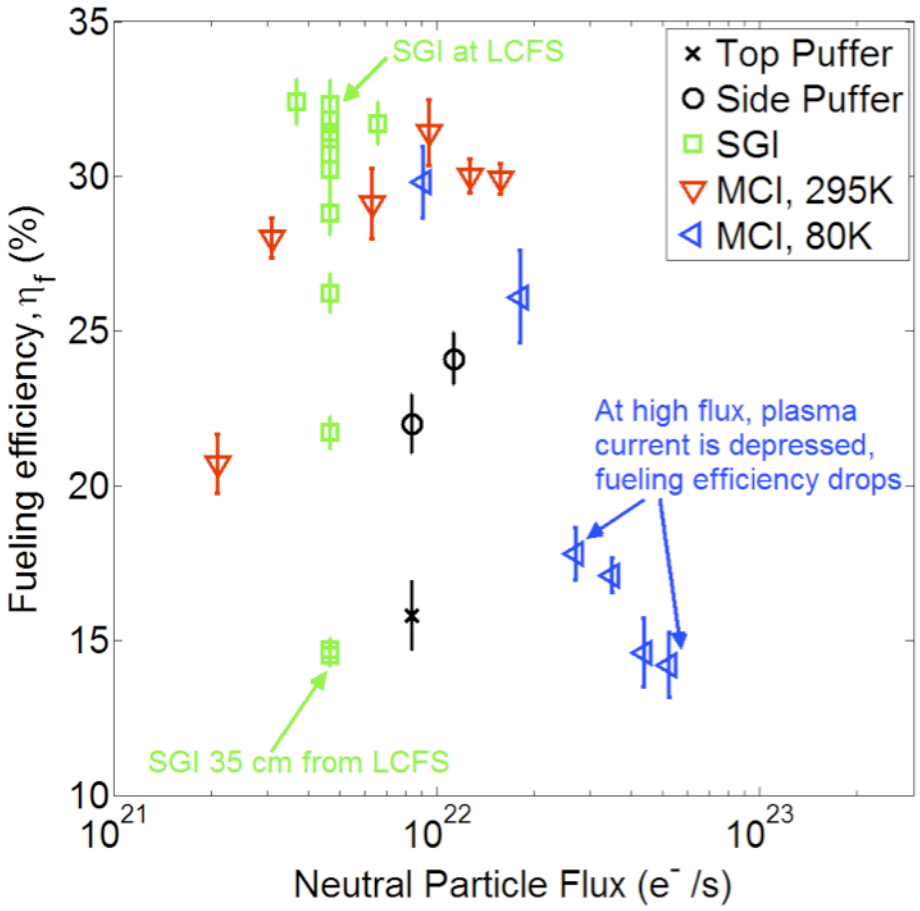
SGI at LCFS
Top Puffer
Side Puffer
SGI
MCI, 295K
MCI, 80K
At high flux, plasma current is depressed, fueling efficiency drops
SGI 35 cm from LCFS
Fueling efficiency, η_f (%)
Neutral Particle Flux (e^- /s)
35
30
25
20
15
10
10^{21}
10^{22}
10^{23}

Figure 5

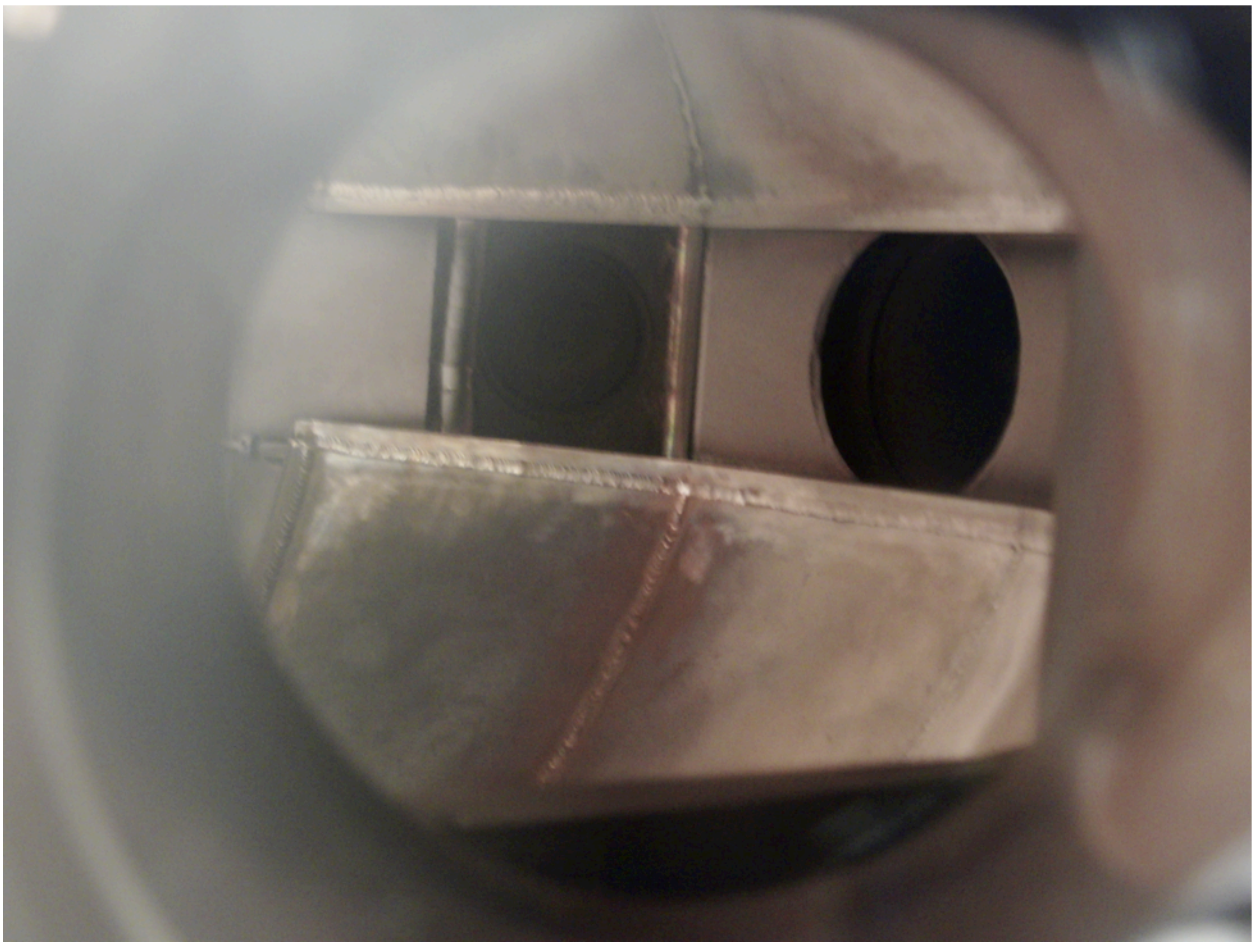

Figure 6

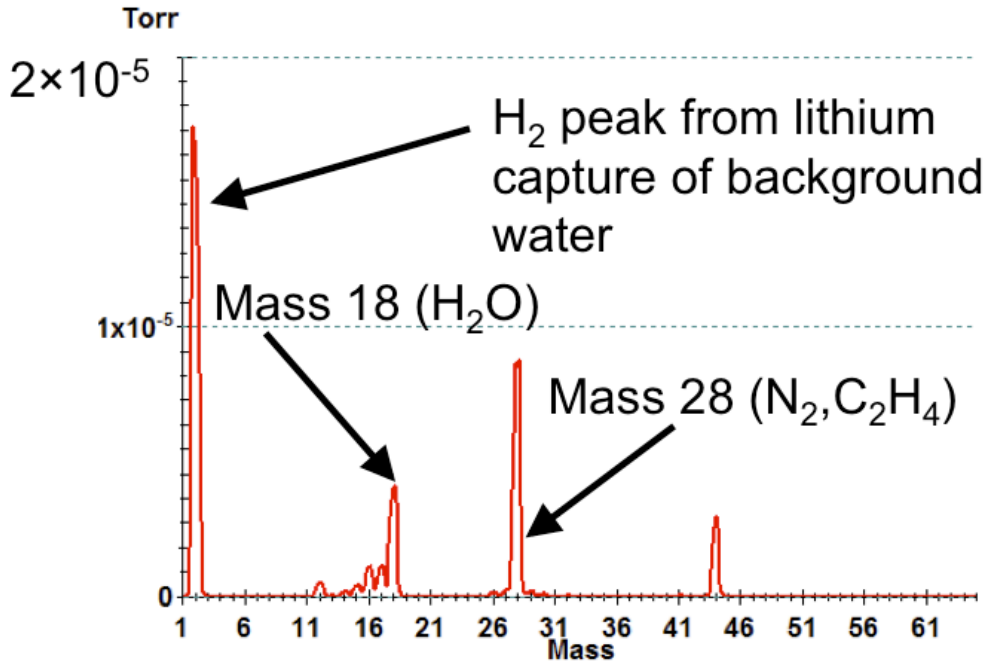
Torr
2×10-5
1x10-5
0
H2 peak from lithium capture of background water
Mass 18 (H2O)
Mass 28 (N2,C2H4)
1
6
11
16
21
26
31
36
41
46
51
56
61
Mass

Figure 7

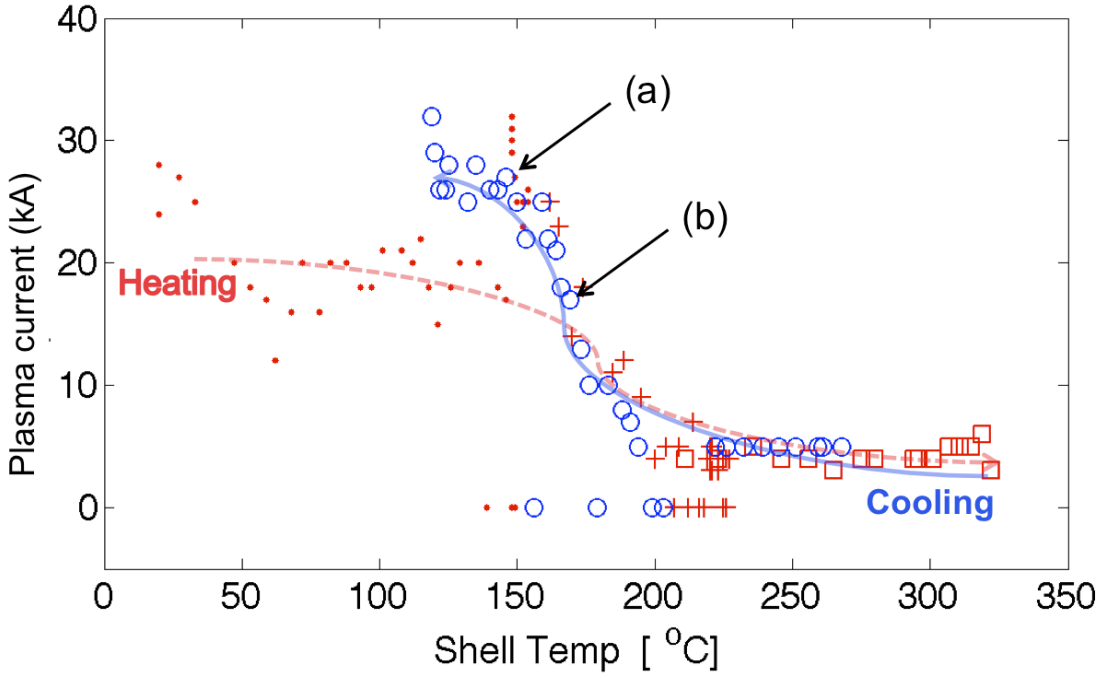
40
30
20
10
0
Plasma current (kA)
(a)
(b)
Heating
Cooling
0
50
100
150
200
250
300
350
Shell Temp [°C]

Figure 8

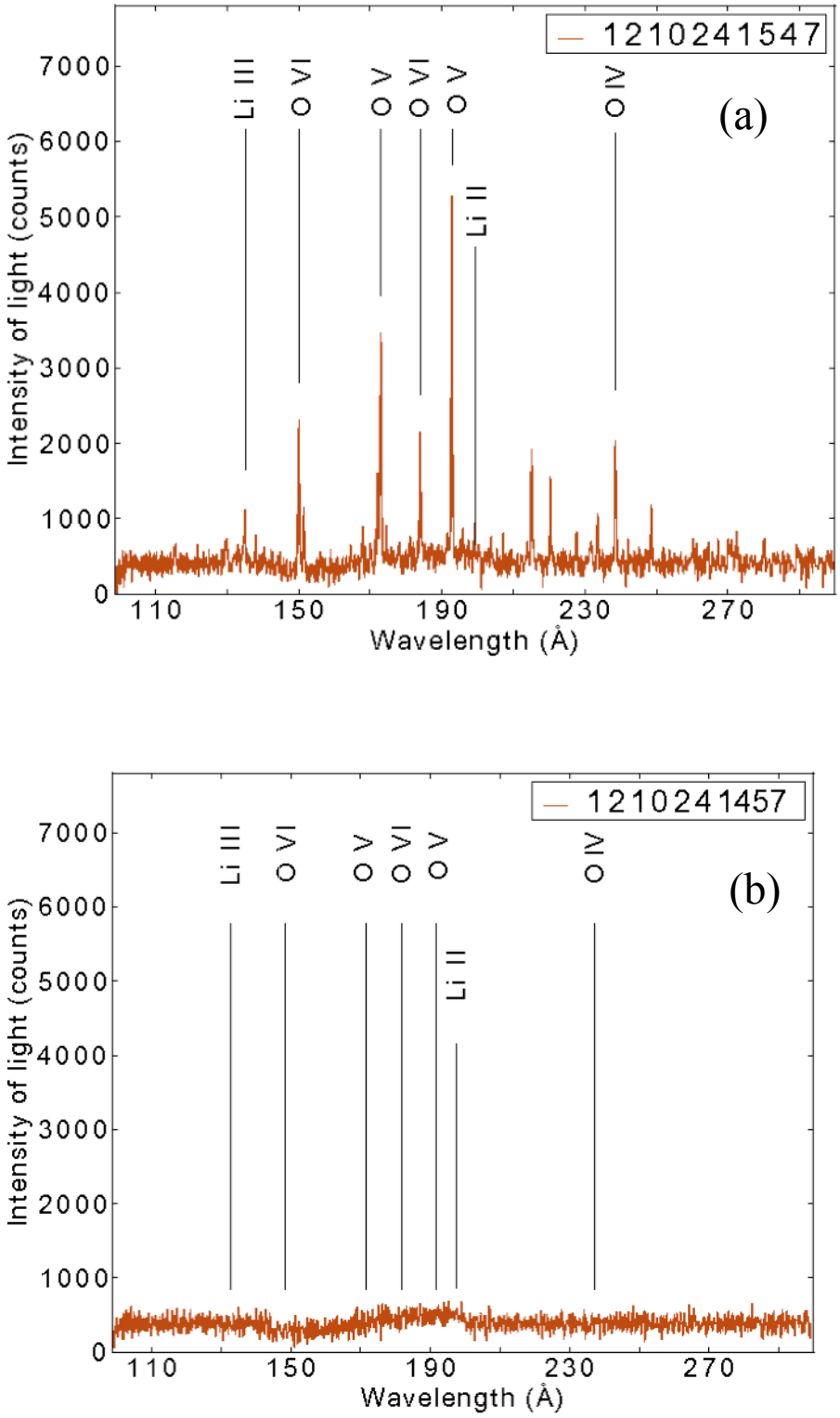
1210241547
Li III
O VI
O V
O VI
O V
Li II
O IV
(a)
Intensity of light (counts)
Wavelength (Å)
1210241457
(b)

Figure 9

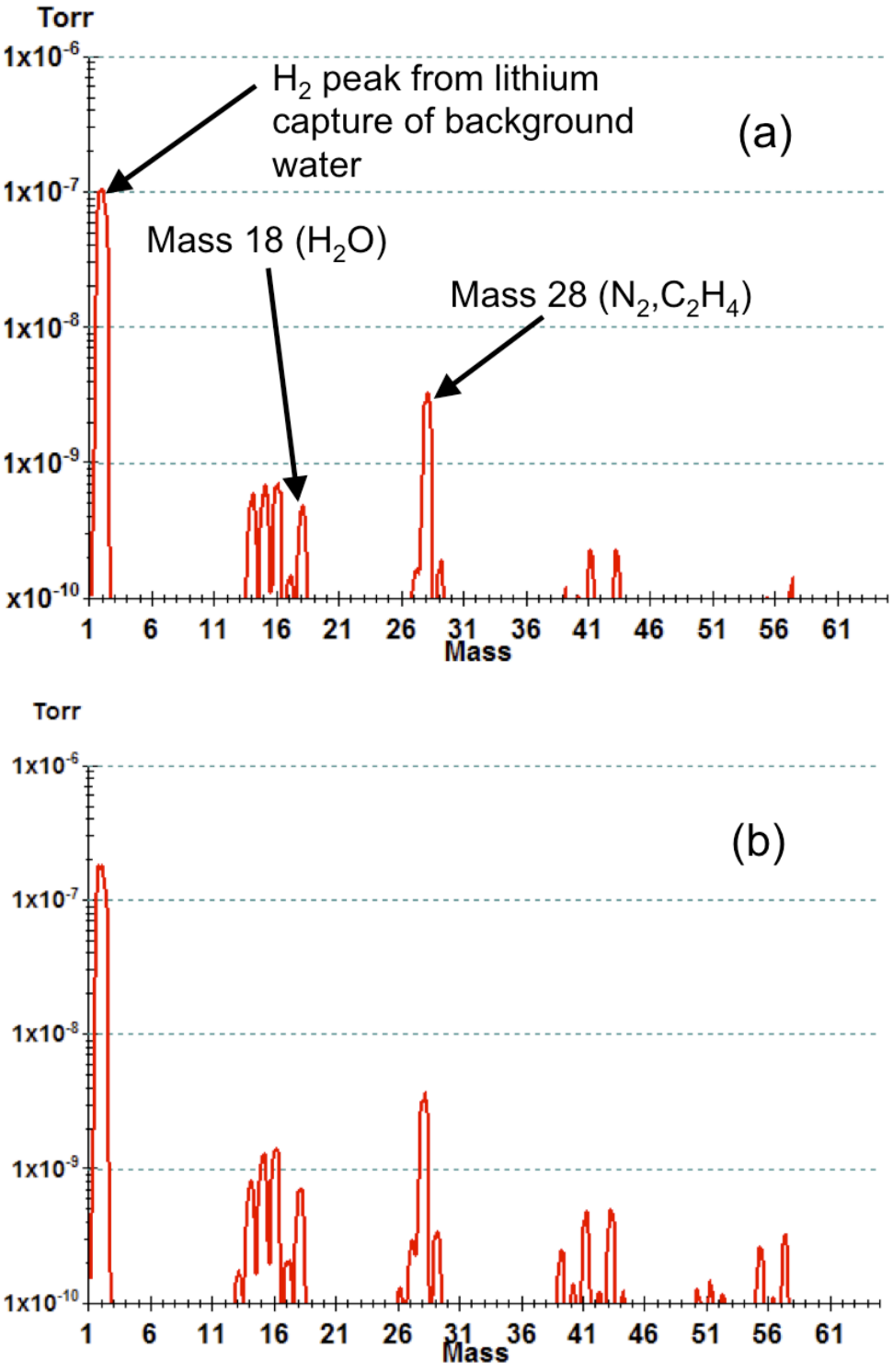
Torr
1x10-6
1x10-7
1x10-8
1x10-9
x10-10
H2 peak from lithium capture of background water
(a)
Mass 18 (H2O)
Mass 28 (N2,C2H4)
1 6 11 16 21 26 31 36 41 46 51 56 61
Mass
Torr
1x10-6
1x10-7
1x10-8
1x10-9
1x10-10
(b)
1 6 11 16 21 26 31 36 41 46 51 56 61
Mass

Figure 10

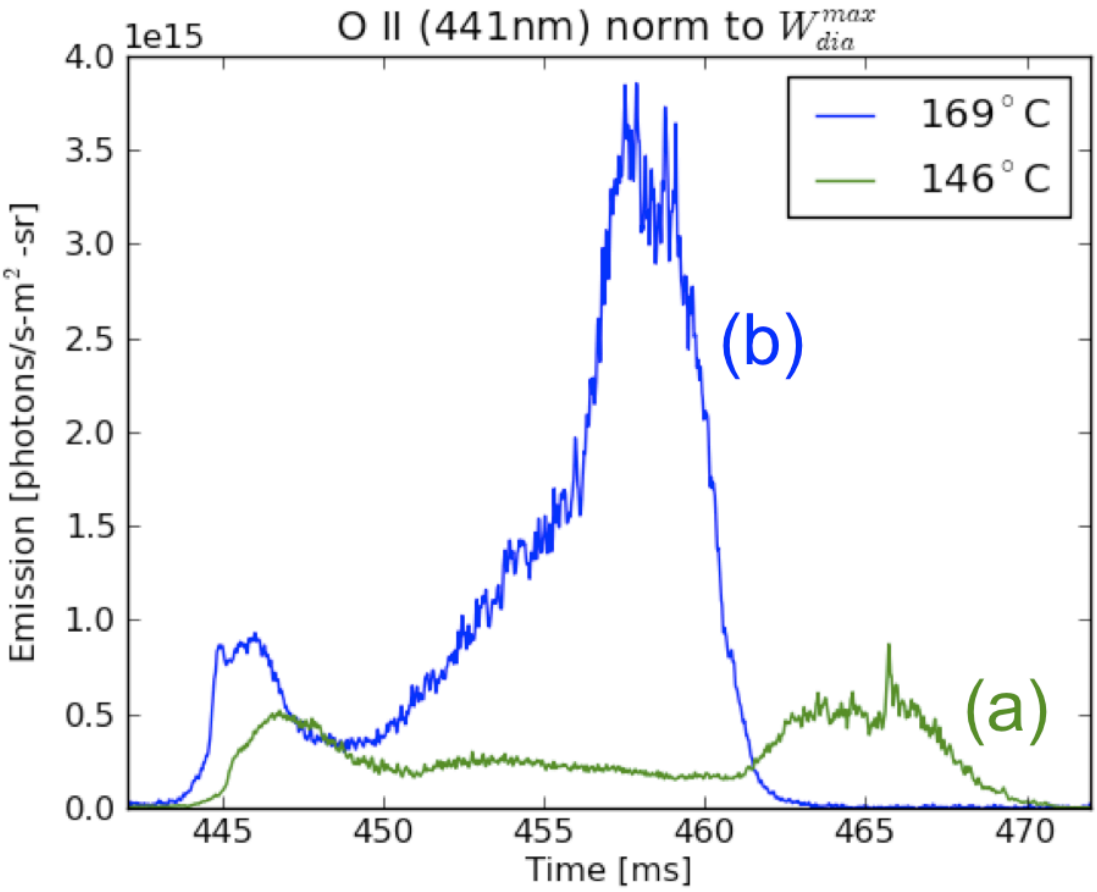
O II (441nm) norm to W_{dia}^{max}
1e15
4.0
3.5
3.0
2.5
2.0
1.5
1.0
0.5
0.0
Emission [photons/s-m^2 -sr]
445
450
455
460
465
470
Time [ms]
169°C
146°C
(b)
(a)

Figure 11

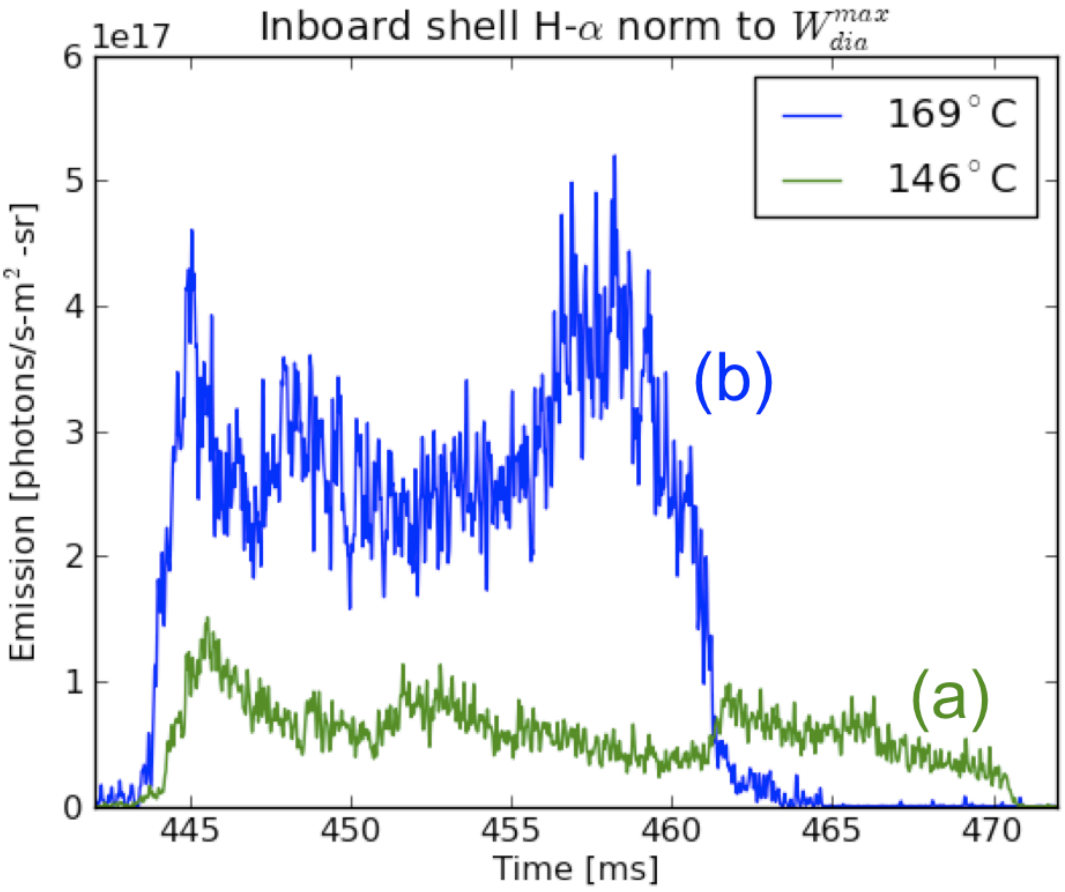
Inboard shell H-α norm to W_{dia}^{max}
1e17
6
5
4
3
2
1
0
Emission [photons/s-m^2-sr]
445
450
455
460
465
470
Time [ms]
169°C
146°C
(b)
(a)

Figure 12

The Princeton Plasma Physics Laboratory is operated
by Princeton University under contract
with the U.S. Department of Energy.

Information Services
Princeton Plasma Physics Laboratory
P.O. Box 451
Princeton, NJ 08543

Phone: 609-243-2245
Fax: 609-243-2751
e-mail: pppl_info@pppl.gov
Internet Address: http://www.pppl.gov